Submicrometer Coherent Neutron Beam Production Using a Thin-Film Waveguide

F. Pfeiffer,[1,2] V. Leiner,[1,3] P. Høghøj,[1,4] and I. Anderson[1]

[1]*Institut Laue-Langevin, B.P. 156, 38042 Grenoble Cedex 9, France*
[2]*Universität des Saarlands, Im Stadtwald 38, 66041 Saarbrücken, Germany*
[3]*Ruhr-Universität Bochum, 44780 Bochum, Germany*
[4]*Xenocs SAS, 19, rue Francois Blumet, 38360 Sassenage, France*

(Received 29 August 2001; published 22 January 2002)

We have experimentally demonstrated that planar neutron waveguides can be used as resonant beam couplers to efficiently produce a coherent neutron line source with cross sections in the submicrometer range. The Fraunhofer far-field diffraction pattern of the first three resonance modes was measured and found to be in excellent agreement with the theoretical model. Our measurements confirm that an excited exiting mode is fully coherent in the direction perpendicular to the surface of the thin-film coupler and may therefore be used for applications of interest to a broad user community in biochemical and semiconductor nanosciences such as static and time-resolved coherent speckle experiments or phase-contrast imaging.

DOI: 10.1103/PhysRevLett.88.055507 PACS numbers: 61.12.–q, 03.75.Be

Neutron diffraction, spectroscopy, and imaging using beam sizes in the submicrometer range are rapidly evolving fields of research. Progress is fueled not only by the availability of novel neutron optics, such as microcollimators, supermirrors, or focusing monochromators, but also by the urgent need for characterization tools that meet the demands of the advances in biochemical and semiconductor nanoscience. During recent years the planar thin-film *x-ray* waveguide structures have been developed and proven to deliver coherent beams efficiently with cross sections in the submicrometer range and with precisely defined properties of divergence and coherence [1–5]. They have been used for submicrometer resolved one-dimensional projection phase-contrast microscopy, microdiffraction, enhanced diffuse scattering, depth profiling of incorporated nanocomposites, and for providing complex far-field diffraction patterns [6–10]. However, for many applications, the achieved x-ray based results (in particular for effects related to magnetism) are limited by the x-ray optical properties of materials. Thus the use of appropriate neutron investigation techniques combined with neutron optical devices with the ability to prepare submicrometer beam sizes would be desirable or even indispensable.

The simple use of slits to define a submicrometer neutron beam width in the range of 100–5000 Å is, however, both difficult and inefficient for various reasons. First, suitable slit materials (like, for instance, B4C or Cd) cannot be processed with the required accuracy to sufficiently avoid diffraction at the slits of the primary beam, which is particularly important when aiming at the preparation of submicrometer beam cross sections. Second, the use of slits would also be extremely inefficient, since only a small fraction of the original beam could then be used. Other submicrometer focusing neutron optics, such as, for instance, Fresnel lenses, microcollimators, or bend crystal optics, are limited by the achievable structural sizes of current nanolithographic techniques, general neutron optical properties of the materials, or the quality of fabrication.

Analogous to the application of prism film couplers to couple visible light into fiber-optical systems, Feng and co-workers [1,2] alternatively proposed the use of a similar resonant beam coupling (RBC) device for neutrons. With this device neutrons can be coupled into a thin guiding layer, guided, and then decoupled under certain conditions [11,12].

Contrary to this approach, where both coupling and decoupling of neutrons was achieved through the surface of the device, we will show in this Letter that specially designed and optimized neutron RBCs (in the following simply called "waveguides") can be used to extract the propagating neutrons at the end of the guide with precisely defined properties of divergence, amplitude, and phase. Since we still couple in through the surface of the device, it is possible to considerably increase the flux throughput compared to a pair of slits of the same width.

Figure 1 shows a schematic diagram of a waveguide structure consisting of a guiding layer of a material with a low neutron scattering length density (such as carbon) with an index of refraction, n_1, sandwiched between a comparably thin cap layer and a rather thick bottom layer of a material with a high neutron scattering length density (such as nickel) and refractive index n_2 [13]. Typical values for the thickness of the cap layer, the guiding layer, and the bottom layer are 30–100 Å, 200–5000 Å, and 500–1000 Å, respectively.

To gain an understanding of the mode excitation and waveguide properties, we have calculated the internal (and external) neutron wave function $|\Psi(\alpha_i, z)|^2$ as a function of structural and geometric parameters (layer thickness, composition and density, interface roughness, angle of incidence, and neutron energy) by a transfer matrix algorithm similar to the one used in the case of optical waveguides [14]. Equivalently, but numerically rather slow, one

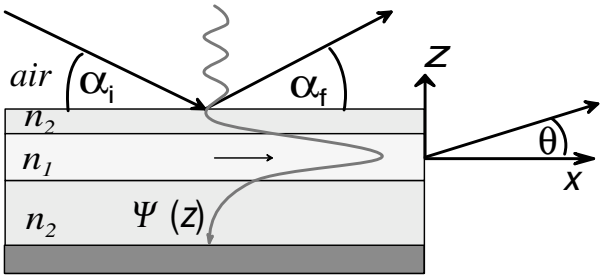

FIG. 1. A sketch of a neutron resonant beam coupling waveguide device. The impinging neutron beam creates a standing wave-field distribution, which excites a resonantly enhanced quasimode inside the structure (see text).

can use a neutron adapted version of the well-known Parratt formalism for such calculations [15]. Figure 2 shows the resulting depth profiles $|\Psi(\alpha_i, z)|^2$ of the resonance modes ψ_0 (excited at $\alpha_{i,0} = 0.357°$), ψ_1 ($\alpha_{i,1} = 0.387°$), and ψ_2 ($\alpha_{i,2} = 0.421°$) of such a calculation for a 52 Å Ni/1410 Å C/490 Å Ni/Si waveguide. The calculations were carried out for a neutron wavelength of $\lambda = 4.4$ Å. The values for the refraction indices, layer thicknesses, and roughness were obtained through x-ray and neutron reflectivity measurements on the fabricated device. As expected, the excitation of resonant modes appears for a set of nearly discrete values of α_i in a range between the critical angle of the guiding layer, $\alpha_{c1} = \sqrt{2\delta_1} \sim 0.348°$, and $\alpha_{c2} = \sqrt{2\delta_2} \sim 0.436°$ (the critical angle of the top and bottom layers). Importantly, the resonant enhancement of $|\Psi(\alpha_i, z)|^2$ with respect to the amplitude of the incident beam can reach a factor of almost 2 orders of magnitude for $\alpha_{i,0} = 0.357°$. The fact that the lowest order mode excitation is the strongest excitation is not a general rule, but a result of the chosen structural properties. By changing the structural properties it is thus possible to favor, for instance, the second or third order mode excitation. Furthermore our simulations showed that the interfacial

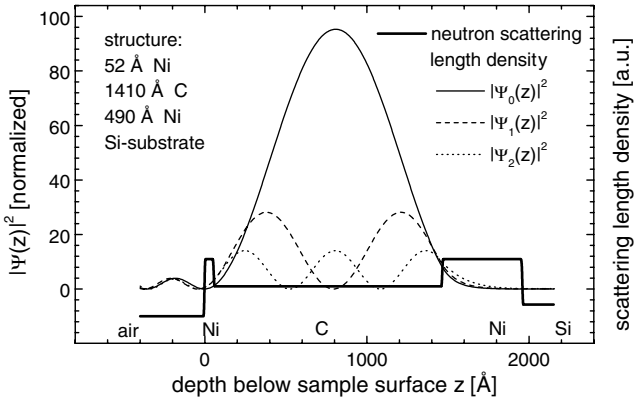

FIG. 2. Calculated neutron wave functions $|\Psi_m(z)|^2$ as a function of depth z of the first three resonance modes (Ψ_0, Ψ_1, and Ψ_2) in a 52 Å Ni/1410 Å C/490 Å Ni/Si substrate neutron waveguide. The bold black line shows the neutron scattering length density in the multilayer stack.

roughness does not alter the intensity values significantly since the product of the rms roughness, σ, and the internal wave vector, k_z', remains small, as long as σ does not far exceed 15 Å.

At the end of the structure, the neutrons trapped in the guiding layer exit the thin-film structure, leading to a beam of high spatial coherence (in the z direction) with a vertical width corresponding to the thickness of the guiding layer and a divergence given by the FWHM of the Fourier transform of the excited standing wave field. Efficient decoupling through the end of the device occurs, if the footprint of the beam is separated from the edge of the sample not much farther than the active coupling length, which was our case (~1200 μm) [16]. The divergence and shape of the exiting guided mode, the angular acceptance, and the absolute number of supported modes can all be controlled by the structural and geometric parameters and can be varied within a certain range [5]. Finally, the far-field pattern $I(\theta)$ of the different modes can be calculated from the complex neutron wave function inside to yield [17]

$$\mathcal{I}_m(\theta) = \mathcal{I}_0 \left| \int_{-\infty}^{+\infty} \Psi_m(z) e^{ik_0 \sin(\theta) z}\, dz \right|^2, \qquad (1)$$

where Ψ_m are the wave functions for angles of incidence $\alpha_{i,m}$ corresponding to the mth order mode excitation (in our case, $\alpha_{i,0} = 0.357°$, $\alpha_{i,1} = 0.387°$, and $\alpha_{i,2} = 0.421°$) [18]. Note that, for neutrons, this equation has to be modified to account for an incoming beam divergence, a certain $\Delta\lambda/\lambda$, and a given detector resolution. This can be done in a quite straightforward way and is not shown here for the sake of simplicity.

To demonstrate the effects calculated above experimentally, a series of differently designed neutron waveguides was fabricated at one of the sputtering facilities at the ILL by using a dc magnetron sputtering process. The samples were measured on the ADAM [19] neutron reflectometer using a pyrolitic graphite monochromator adjusted to give a neutron wavelength of 4.4 Å with an energy spread of $\Delta\lambda/\lambda \simeq 0.7\%$. We used a beam size at the sample of 20 mm(vert) × 0.5 mm(hor), where the sample's surface normal corresponded to the horizontal direction. A ^{3}He detector was mounted on the detector arm at a distance of 1660 mm. For our most efficient waveguide, reflectivity measurements (not shown here) combined with subsequent fitting procedures based on the typical densities of sputtered Ni and C resulted in the following structural properties: 52 Å Ni/1410 Å C/490 Å Ni layers on Si substrate, average rms roughness $\sigma = 12$ Å, and a 16 Å NiO_x oxidation layer on top.

According to the simulations above, the waveguided beam is expected to exit the device at the end in a direction parallel to the surface ($\alpha_f \cong \theta = 0$) when the angle of incidence matches the resonance condition of one of the modes [18]. This can be proven experimentally by measuring the intensity integrated over ±0.1° (adjustable using properly set detector slits) around the horizon ($\alpha_f = 0$) as

a function of the angle of incidence α_i. The result of such a measurement, shown together with the measured and simulated reflectivity ($\alpha_i = \alpha_f$) in that angular range, is plotted in Fig. 3. The measured intensity of the waveguided mode peaks at values of the angle of incidence corresponding to the expected mode excitation angles of Ψ_0, Ψ_1, and Ψ_2 (see again Fig. 2). This already clearly demonstrates that an observable flux can be extracted out of the thin-film waveguide at the end [20].

To study the Fraunhofer diffraction pattern of the different excited modes in detail, we have measured the intensity distribution as a function of α_f for different angles of incidence corresponding to the mth order mode excitation. Figure 4 shows these results (open circles) together with the calculations (line) based on Eq. (1), where an energy spread of $\Delta\lambda/\lambda = 0.7\%$, an incoming beam divergence of 0.015°, and a detector resolution of 0.02° have been included.

Importantly, the only fitting parameter used was the maximum intensity, I_0, from which information about the efficiency or gain can now be deduced. The latter value is defined by the ratio between the integrated flux exiting the waveguide (directly measurable by properly integrating over the divergent far-field pattern) and the flux that one would obtain using a pair of hypothetical slits to prepare a neutron beam with the same cross section as the thickness of the guiding layer and a divergence corresponding to the angular acceptance of the excited mode. Our most efficient waveguide yielded a gain value of 17 ± 3, which is in the same range as the enhancement for x-ray waveguides after several years of development. Note that this gain value is of course not in contradiction to Liouville's theorem, since the waveguide mainly acts as a coherence filter and as an optical device, which transforms the phase space of the incoming beam into an exiting beam with significantly reduced cross section and increased divergence.

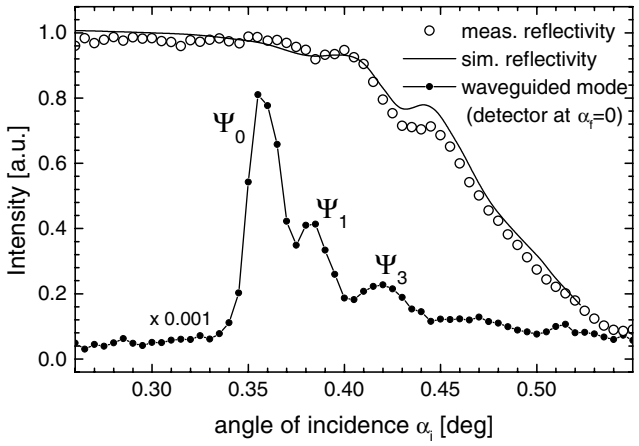

FIG. 3. Upper curve: simulated (line) and measured (open circles) reflectivity in the region of total reflection. Lower curve: measured intensity as a function of α_i with the detector fixed at $\alpha_f = 0$ to detect the resonantly excited, horizontally exiting waveguided modes (full circles connected by line).

A comparison of the obtained gain value with a theoretical limit is, however, rather difficult since these estimations should include both the divergence and the energy spread of the incoming beam, as well as losses due to interface roughness, small-angle scattering in the guiding layer, and mode-mixing effects. However, as an estimate, gain values of more than 100 are achievable with further optimized structures and improved, adapted beam-line optics, as has recently been proven in the case of x rays [4].

As for the coherence properties of the exiting waveguided beam, the fact that the simulation matches almost perfectly with the measured data already confirms the high degree of transverse coherence of the wave field in the direction perpendicular to the surface of the guide, since Eq. (1) is true only for a fully coherent beam propagation [21]. For a more precise determination of the degree of the transverse coherence of a given beam, one usually employs a standardized diffraction grating or a pinhole and deduces the degree of coherence from the visible interference fringes. However, rather than following exactly this procedure we fabricated waveguides comprising several guiding layers and thus incorporated the source and the "standardized diffraction grating" into one device. The resulting excited internal resonant enhanced neutron wave field can again be calculated in the same manner as described above. However, due to mode splitting, the shape and phase of the neutron wave functions in such a device are more complicated and will be discussed in detail elsewhere [22]. In a simplified view, low order excitation modes of such a multiple guiding layer waveguide can be considered as a source of several, distinct, coherent beams emerging with the same phase from the different guiding layers. We measured the resulting far-field diffraction pattern (Fig. 5) of such a device (with ten 469 Å carbon

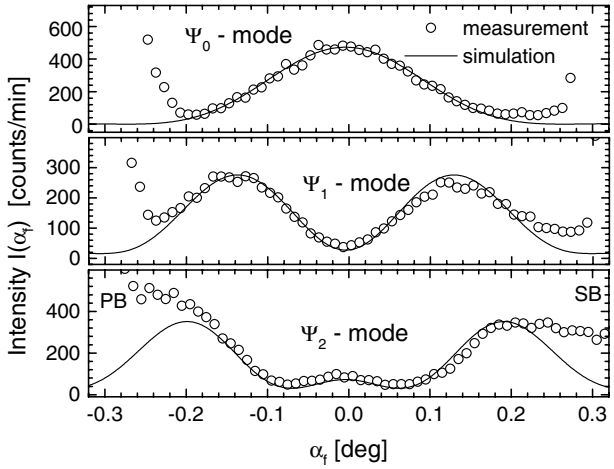

FIG. 4. Measured (circles) and calculated (lines) far-field pattern of the excited Ψ_0 ($\alpha_{i,0} = 0.357°$), Ψ_1 ($\alpha_{i,0} = 0.387°$), and Ψ_2 ($\alpha_{i,0} = 0.421°$) modes. The rise of the measured intensity towards greater values of α_f is due to the tails of the primary beam (PB) and the specular reflected beam (SB), having their maxima at $\alpha_f = \pm\alpha_i$.

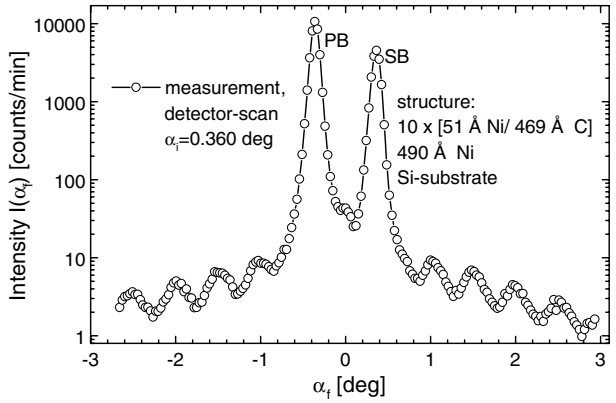

FIG. 5. Measured far-field interference pattern of a multiple guiding layer waveguide with the angle of incidence fixed at $\alpha_i = 0.360°$. The high degree of transverse coherence is confirmed by the number and the contrast (logarithmic scaling) of the clearly visible interference fringes.

guiding layers) and observed high contrast interference fringes, which did not show any significant broadening within the first few orders. Clearly, this again confirms the high degree of coherence of the exiting mode, particularly since the number of measured fringes was not limited by their intensity, rather by the surface area of the used two-dimensional detector.

In conclusion, we have shown that using the resonant beam coupling principle for thin-film neutron waveguides allows for the efficient production of a coherent neutron line source with a beam cross section in the submicrometer range. The Fraunhofer far-field diffraction pattern of the excited modes was measured with unprecedented quality, resolution, and intensity. We take the good agreement with the theoretical description, in the case of a single guiding layer waveguide, together with the number and contrast of the observed interference fringes, in the case of a multiple guiding layer waveguide, as experimental confirmation of the high degree of transverse coherence of the exiting beam.

Many applications using these devices for submicrometer spatially resolved coherent microdiffraction, (phase-contrast) projection microscopy, or microinterferometry can be envisioned. In this way information on the local, nanoscale nuclear scattering density can be projected onto macroscopic area detectors. The applications opened up by this novel technique are of interest to a broad user community in biochemical and semiconductor nanosciences. Further progress is expected from improved material compositions combined with adapted prefocusing optics. The application of these devices at next generation neutron sources may then even lead to efficient two-dimensional focusing devices in the future.

We thank W. Graf, K. Ben-Saidane, and V. Schönherr for their technical help and T. Salditt for a series of fruitful discussions.

[1] Y. P. Feng, H. W. Deckmann, and S. K. Sinha, Appl. Phys. Lett. **64**, 1 (1993).
[2] Y. P. Feng *et al.,* Phys. Rev. Lett. **71**, 537 (1993).
[3] M. J. Zwanenburg *et al.,* Phys. Rev. Lett. **82**, 1696 (1999).
[4] W. Jark, A. Cedola, S. Di Fonzo, and M. Fiordelisi, Appl. Phys. Lett. **78**, 1192 (2001).
[5] F. Pfeiffer, T. Salditt, P. Høghøj, I. Anderson, and C. David, SPIE Int. Soc. Opt. Eng. **4145**, 193 (2001).
[6] S. Lagomarsino *et al.,* Appl. Phys. Lett. **71**, 2557 (1997).
[7] S. Di Fonza *et al.,* Nature (London) **403**, 638 (2000).
[8] M. Müller, M. Burghammer, D. Flot, C. Riekel, C. Morawe, B. Murphy, and A. Cedola, J. Appl. Crystallogr. **33**, 1246 (2000).
[9] F. Pfeiffer, U. Mennicke, and T. Salditt, J. Appl. Crystallogr. (to be published).
[10] F. Pfeiffer, T. Salditt, P. Hoghoj, and I. Anderson, Phys. Rev. B **62**, 16 939 (2000).
[11] Y. P. Feng *et al.,* Phys. Rev. B **49**, 10 814 (1994).
[12] Contrary to the case of visible light, where the index of refraction is greater than 1, no prism is needed for neutrons, since the index of refraction is below 1.
[13] The refraction index for neutrons is given as $n = 1 - \delta - i\beta$, where δ (β) is proportional to the real (imaginary) part of the neutron scattering length density of the material.
[14] M. R. Shenon, K. Thyagarajan, and A. K. Gatah, J. Lightwave Technol. **LT-6**, 1285 (1988).
[15] L. G. Parratt, Phys. Rev. **95**, 359 (1954).
[16] P. K. Tien and R. Ulrich, J. Opt. Soc. Am. **60**, 1325 (1970).
[17] D. Marcuse, *Theory of Dielectric Optical Waveguides* (Academic, New York, 1974).
[18] For all practical purposes the angle θ can be assumed to be equal to α_f, since this error is much smaller than other uncertainties such as, for instance, the instrumental resolution or even the accuracy of the simulation.
[19] ADAM: neutron reflectometer operated by the Ruhr-Universität Bochum at the ILL, Grenoble.
[20] Note that, due to weak absorption of neutrons inside the guide, hardly any cusps in the plateau of total external reflection are observable, in contrast to what is usually observed in x-ray waveguide experiments (see [5] for some examples).
[21] The longitudinal coherence length is not affected by the device and is still given as $\lambda^2/\Delta\lambda$ (see also [17]).
[22] F. Pfeiffer, V. Leiner, P. Høghøj, and I. Anderson, SPIE Proceedings 4109-11 (to be published).